Computation & theory

Ab initio molecular dynamics studies on the ignition and combustion mechanisms, twice exothermic characteristics, and mass transport properties of Al/NiO nanothermite

Shenghua Feng[1], Guolin Xiong[1], and Weihua Zhu[1,*] (ID)

[1] *Institute for Computation in Molecular and Materials Science, School of Chemical Engineering, Nanjing University of Science and Technology, Nanjing 210094, China*

ABSTRACT

Ab initio molecular dynamics was used to simulate the ignition and combustion reaction process of the Al/NiO nanothermite. The exothermic characteristics and the role of oxygen migration in the whole reaction were disclosed. The results suggest that the primary and secondary heat release are mainly caused by the interfacial and bulk thermite reaction, respectively. The interfacial oxygen migration and the breaking of Ni–O bonds cause the initial ignition. The destruction of the bulk NiO lattice is the precursor process of the secondary heat release and retards the rapid thermite reaction. The ^{18}O isotope leads to a lower oxygen mass transport rate, having a great influence on the ignition delay time and reaction progress. The metal–oxygen flip mechanism ensures the continuous propagation of the thermite reaction. Our work may be helpful for understanding the reaction mechanisms of the metal/metal oxide thermites and optimizing the formulation design and performance of the nanothermites.

Introduction

Nanothermite is an energetic material formed by an intimate contact of an oxidant and a reductant (usually a metal oxide and a metal) on the nanometer scale. The nanoscale treatment of traditional micron-sized thermite can greatly improve its reactivity. Nanothermite has the advantages of high energy release rate, high combustion rate, and low ignition temperature [1–5]. Therefore, it can be applied in a wide range of fields, such as welding [6], gas generators [7, 8], microthrusts [9], microinitiators [1, 10] etc. Especially, its full compatibility with micro-electromechanical systems (MEMS) makes it be an ideal component developed in nano-energetics-on-a-chip systems [11, 12]. The quantity of gases generated by the Al/NiO thermite is 2% from Al/CuO, 7.7% from

Handling Editor: Yaroslava Yingling.

Address correspondence to E-mail: zhuwh@njust.edu.cn

Al/Fe$_2$O$_3$, 2.3% from Al/Bi$_2$O$_3$, and 4.5% from Al/MoO$_3$ in terms of mol/g, so it is very suitable to be used as a microinitiator that requires less component vibration and little flow disturbance [1, 10, 13, 14]. In addition, the onset temperature of Al/NiO thermite was reported to be lower than that of Al/CuO thermite [15]. Due to these advantages, the Al/NiO thermite has been attracting great attention.

The Al/NiO thermite was already prepared by physical mixing [15, 16], sputtering deposition [1, 17], vacuum filtration [18], thermal evaporation [19], and electrophoretic deposition [10]. In recent years, some theoretical calculations were performed to study the reaction of the Al/NiO nanothermite. Fathollahi et al. [20, 21] carried out reaction force field (ReaxFF) molecular dynamics (MD) simulations on the Al/NiO system under NPT ensemble and obtained the reaction temperature according to the sudden change of volume and potential energy. Zeng et al. [22] studied the effects of equivalence ratio and onset temperature on the thermite reaction of the film-honeycomb Al/NiO nanothermite under NVE ensemble by ReaxFF MD simulations. Wen et al. [16] used X-ray diffraction (XRD) to detect the presence of AlNi in the reaction products and verified the experimental results by ab initio MD (AIMD) simulations.

Many studies have centered on the mechanism of aluminum nanoparticle oxidation and thermite reaction. Rai et al. [23] pointed out that the oxidation of aluminum nanoparticle has two regimes. Below the melting point of aluminum, the oxidation was caused by the diffusion of O through the oxide layer. Above the melting point, both Al and O passed through the oxide shell with a faster rate. The diffusion-controlled mechanism was verified by Chowdhury et al. [24] based on the ignition of Al/CuO nanothermite. Henz et al. [25] revealed that the diffusion of Al cation is driven not only by the volume expansion of the Al core, but also mainly by the induced electric field of the oxide layer. Levitas et al. [26–28] proposed that the melt dispersion mechanism that the ignition or reaction of the Al nanoparticles occurs due to the spallating of the oxide shell caused by the molten aluminum core under very high heating rate (above 10^6 K/s). Differential scanning calorimetry (DSC) and thermogravimetric analysis (TGA) are widely used to characterize the thermal reaction properties of the nanothermites. Some experiments have revealed that the reaction of the Al/NiO nanothermite presents a twice heat release phenomenon [1, 15, 17, 19]. However, few researchers have studied the formation mechanism of the twice exothermic peaks during the Al/NiO thermite reaction, especially for these thermites with nanomultilayer morphology. In addition, the ignition and combustion mechanisms of the nanothermites have been poorly understood at the electronic and atomic levels. Oxygen migration is closely related to the thermite reaction; however, there are few studies put on the influence of oxygen mass transport rate on the thermite reaction. As is well-known, the long ignition delay time and low reaction rate are the factors that limit the application of the nanothermites as energy materials [29]. Therefore, it is very necessary to study the ignition, combustion mechanisms, and exothermic characteristics of the thermites as well as the effect of oxygen mass transport on thermite reaction.

With the improvement of computing power in recent years, the high-level AIMD method has been using in the study of the thermite systems duo to its high calculation accuracy. Shimojo et al. [2, 11] systematically studied the reaction of the Al/Fe$_2$O$_3$ thermite and proposed a metal–oxygen flip mechanism. Tang et al. [30] theoretically analyzed the reaction process and products of the Al/CuO thermite through chemical bonds, average charge, and potential energy. Xiong et al. [31, 32] investigated the reaction process of the Al/CuO thermite under NVT and NVE ensembles and pointed out that the temperature promotes the combustion reaction.

In this work, we performed AIMD simulations on the Al/NiO nanothermite. Gradient heating was used to study its non-isothermal combustion reaction process. To study the influence of oxygen mass transport on the thermite reaction, we used ^{16}O and ^{18}O in the Al/NiO system to probe the mass transport properties. Our main purpose is to reveal the twice heat release phenomenon, the ignition and combustion mechanisms, and the properties oxygen mass transport for the Al/NiO nanothermite.

Computational methods

All DFT calculations were carried out using the projector-augmented-wave (PAW) method [33] implemented in the Vienna Ab Initio Simulation Package (VASP) [34, 35]. The electron exchange–correlation potentials were described using the Perdew

Burke-Ernzerhof (PBE) functional [36] of the generalized gradient approximation (GGA). In order to describe strong electronic correlation for NiO, we adopt spin-polarized DFT + U method [37]. The effective U value of 6.45 eV was chosen for Ni atoms [38, 39].

For Al and NiO bulks, the plane wave energy cutoff was set to 700 eV with a k mesh density of $2\pi0.02$ Å^{-1}. Γ-centered k-mesh was used to achieve Brillouin zones sampling in geometry optimization. The convergence criteria of energy and force was less than 10^{-6} eV and 0.01 eV/Å, respectively. According to X-ray diffraction experimental results, the most exposed crystal planes at the Al/NiO thermite interface are the (111) plane of Al and the (200) plane of NiO [1]. Meanwhile, theoretical results showed that the (100) plane is the most stable crystal plane of NiO [40, 41]. Based on these results, a orthogonal supercell of Al(111)/NiO(100) interface model including 108 atoms (48Al + 30NiO) was built. The aluminum in the system is excessive.

For the interface model, all the atoms were relaxed using an energy cutoff of 500 eV. The k mesh density was set to $2\pi0.03$ Å^{-1}. Self-consistent field was convergence to less than 10^{-5} eV. The relaxation stopped when force on each atom was less than 0.02 eV/Å. Figure 1a displays the relaxed structure of the Al/NiO thermite.

There is a view that if a reaction is self-sustaining, the heating rate should be comparable to the reaction rate [42]. Some computational researches revealed that thermite reaction can completely burn in tens or hundreds of picoseconds [2, 22, 31, 32]. So in our simulations, the temperature put on the systems was linearly risen from 10 to 1500 K by velocity scaling in 45 ps (about 33 K/ps heating rate), following stay in the final temperature (1500 K) for 15 ps in NVT ensemble with Nose–Hoover thermostat [43–45]. In all the AIMD simulations, an energy cutoff of 400 eV, a time step of 1.5 fs, and the convergence threshold of 10^{-5} eV for electronic step's iteration were set. In order to study the influence of oxygen mass transport properties on the thermite reaction, we label oxygen atoms with ^{16}O and ^{18}O. For convenience, the simulations containing ^{16}O and ^{18}O isotope are denoted as "10–1500 K simulations" and "10–1500 K-iso simulations," respectively. Unless otherwise specified, our subsequent discussion and analyses were based on 10–1500 K simulations.
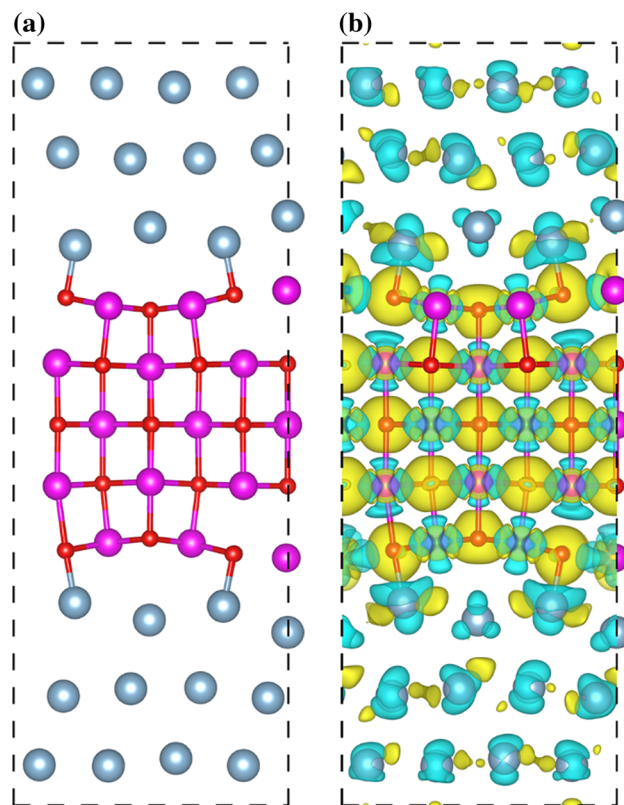

Figure 1 Front view (along x–z plane) of **a** optimized Al/NiO structure and its deformation charge density **b** Al, Ni, and O atoms are colored in light blue, purple, and red, respectively. 0.005 e/Bohr^3 is selected as the value of the isosurface. Cyan and yellow represent the decrease and increase in charge density, respectively.

VESTA [46] program was used to visualize geometric and electronic structures. VMD [47] and VASPKIT [48] programs were explored to process radial distribution function and planar deformation charge density data, respectively.

Results and discussion

Deformation charge density

It can be found from Fig. 1a that the Al atoms at the interface were partially oxidized. This shows that the redox reactions are prone to take place at the interface, which should be avoided in practical applications so that the thermites can store more energy. Figure 1b shows the deformation charge density along the x–z plane for the relaxed Al/NiO thermite. The Al–Al bonds in the Al layers tend to form metallic bonds by sharing electrons. The Ni–O bonds in the NiO layer have electrons localized on the O

atoms and so tend to be ionic bonds. At the interface, we can also observe that the electrons localized on the oxygen atoms result in forming the Al–O ionic bonds. In a word, there are two reasons why Al at the interface is easy to be oxidized. One is that the atoms are in an unstable state due to dangling bonds. The other is that the Al–O bond tends to form ionic bonds.

Figure 2a, c, e and g displays the deformation charge density of the Al/NiO thermite at 0 ps, 15 ps, 30 ps and 45 ps, respectively. We observed that no thermite reaction took place in the time range of 0–15 ps. When the simulation time reaches 30 ps, the geometric and electronic structures of the NiO layers have already destroyed and the thermite reaction has already propagated from the interface to the bulk phase. Furthermore, some Ni atoms penetrate the aluminum oxide film to enter the Al layers and interact with Al to form Al–Ni phase. This phenomenon is consistent with the experimental and theoretical results [13, 16–19, 49]. Finally, NiO is reduced to Ni and tends to aggregate, while some interfacial Ni atoms penetrate into the Al layers where the Al atoms are oxidized to aluminum oxide. The distribution of planar deformation charge density for the Al/NiO along z direction is shown in Fig. 2b, d, f, and h. In the initial stage of the simulations, the electronic structure of the Al/NiO thermite has a highly symmetrical distribution along the atomic layers. With the increasing temperature, the symmetry of the electronic structure is destroyed and the distribution of charge density along the z direction tends to be uniform, which means that the redox reaction propagates in the whole system and the system tends to be disordered.

Potential energy curve

For the simulation in the temperature range of 10–1500 K, as shown in Fig. 3g, we qualitatively divided the whole simulation into five stages according to the change of potential energy in order to grasp the overall trend of the reaction. The first stage (I stage) is in about 0–21.7 ps. In this stage, the potential energy of the Al/NiO system gradually increases. The oxygen atom bonded to Al at the interface begins to migrate to the Al layer at 15.5 ps (as shown in Fig. 3a). There is also a small exothermic peak (where we marked with a red circle) in the potential energy curve which may be very difficult to probe in experiment. As the interfacial Ni–O bond is

broken at the end of I stage, the oxygen atom that initially migrated to the aluminum layer is completely captured by Al. At the same time, the interfacial Ni also begins to migrate to the Al layer (as shown in Fig. S1). This indicates that the Al/NiO thermite is ignited. Through the temperature distribution (as shown in Fig. 3f), we can note that the hot spot area formed at the interface coincides with the area where the oxygens begin to migrate. Owing to the low temperature in this stage, the thermite reaction spreads very slowly.

The second stage (II stage, primary heat release) is in the time range of approximately 21.7–27.2 ps, where the Al atoms mainly interacted with NiO at the interface. The NiO bulk phase still maintains a substantially complete lattice arrangement without participating in the reaction at this stage (as shown in Fig. 3b). So the decrease in the potential energy is relatively less, as shown in Fig. 3g. Meanwhile, it is found in Fig. 3f and h that the temperature at the oxidation front is higher than that in other regions, which allows the reaction to continue propagating. As a result, the original bulk phase becomes the interface.

The third stage (III stage) is in about 27.2–31.5 ps. At this stage, the lattice of the original NiO bulk phase is destroyed (as shown in Fig. 3c), and the thermite reaction is in a state of near stagnation, which is consistent with the change of the potential energy that is almost unchanged (slightly reduced). The fourth stage (IV stage, secondary heat release) is during about 31.5–39.3 ps, and there are mainly the reactions between the destroyed bulk NiO and Al (as shown in Fig. 3d). This stage is the rapid chemical reaction stage of the thermite reaction, and the decrease in the potential energy is significantly greater than that in the II stage, in accordance with the DSC experiments results [1, 17]. The heat release rate in this stage is also obviously greater than that in the second stage. There are mainly three reasons. One is the higher system temperature at this stage. The second may be the melting of Al and the destruction of NiO lattice accelerates the mass transport. Last but not least, the thermite reaction is self-sustaining exothermic reaction and the amounts of Al and NiO participating in the reaction in this stage are greater than those in the interface thermite reaction stage (II stage). After 39.3 ps, the thermite reaction is basically complete, as shown in Fig. 3e.
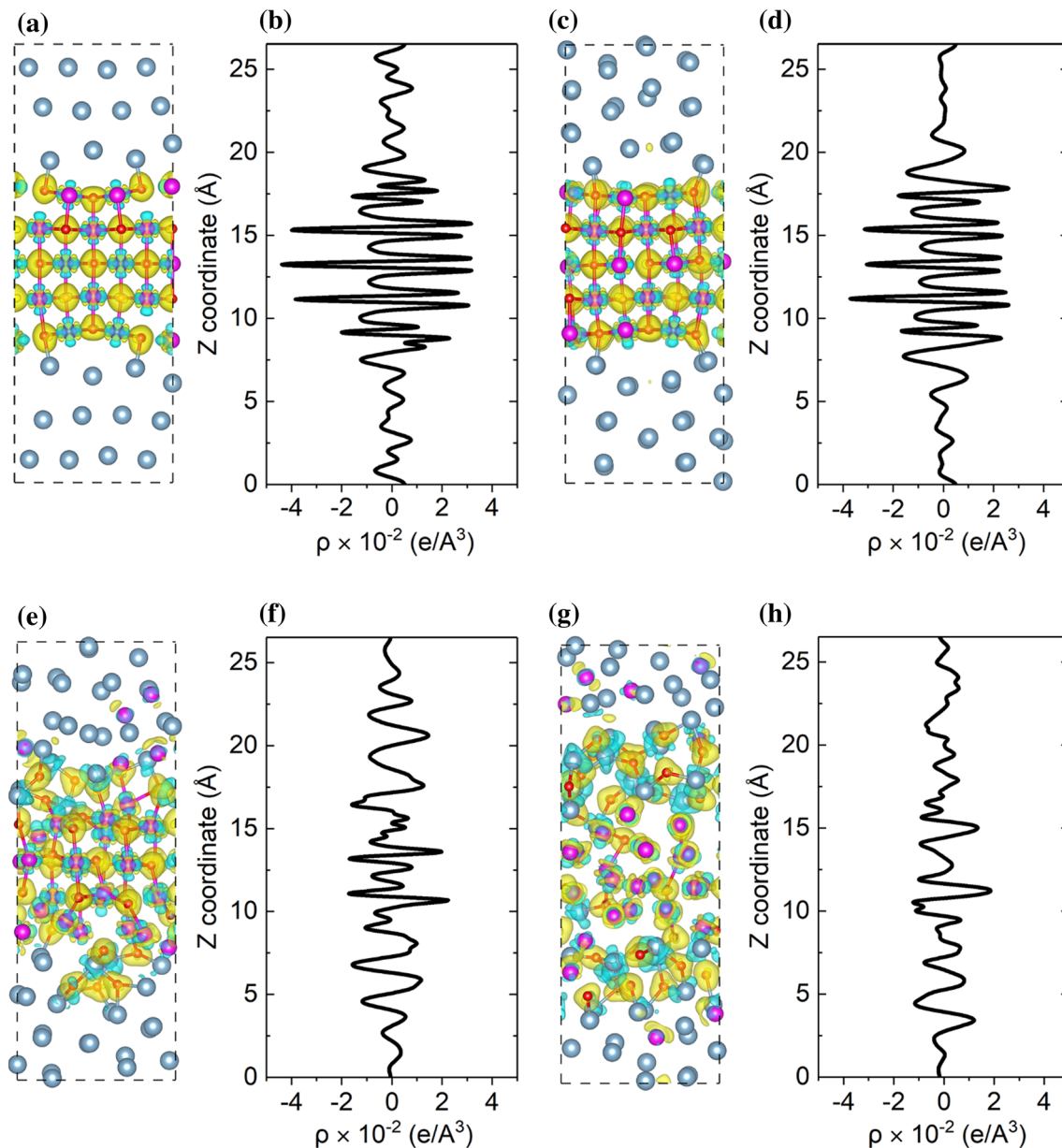
Figure 2 Deformation charge density for the Al/NiO thermite at **a** 0, **c** 15, **e** 30, and **g** 45 ps. Planar average deformation charge density along z direction for the Al/NiO thermite at **b** 0, **d** 15, **f** 30, and **h** 45 ps. Al, Ni, and O atoms are colored in light blue, purple, and red, respectively. 0.012 e/Bohr^3 is selected as the value of the isosurface.

Radial distribution function (RDF) analysis

We divided the Ni atoms into two types (as shown in Fig. S2): Ni in the interface (the NiO atomic layer at the outermost layer of the upper and lower interfaces in the initial structure, denoted as "interfacial Ni") and Ni in the bulk phase (the middle three layers of NiO atomic layer in the initial structure, denoted as "bulk Ni"). The O atoms were also divided in the same way. According to the division of reaction stages in "Potential energy curve" section, we calculated the RDF in each time range. The RDF $g(r)$ and integrated $g(r)$ of the interfacial Ni–O and bulk Ni–O atom pairs during the five reaction stages are separately calculated and shown in Fig. 4. In the chemical reactions of the Al/NiO thermite, there are both the breaking of old chemical bonds (Ni–O) and the formation of new chemical bonds (Al–O). Thus, the RDFs of the interface O–Al and bulk O–Al atom pairs
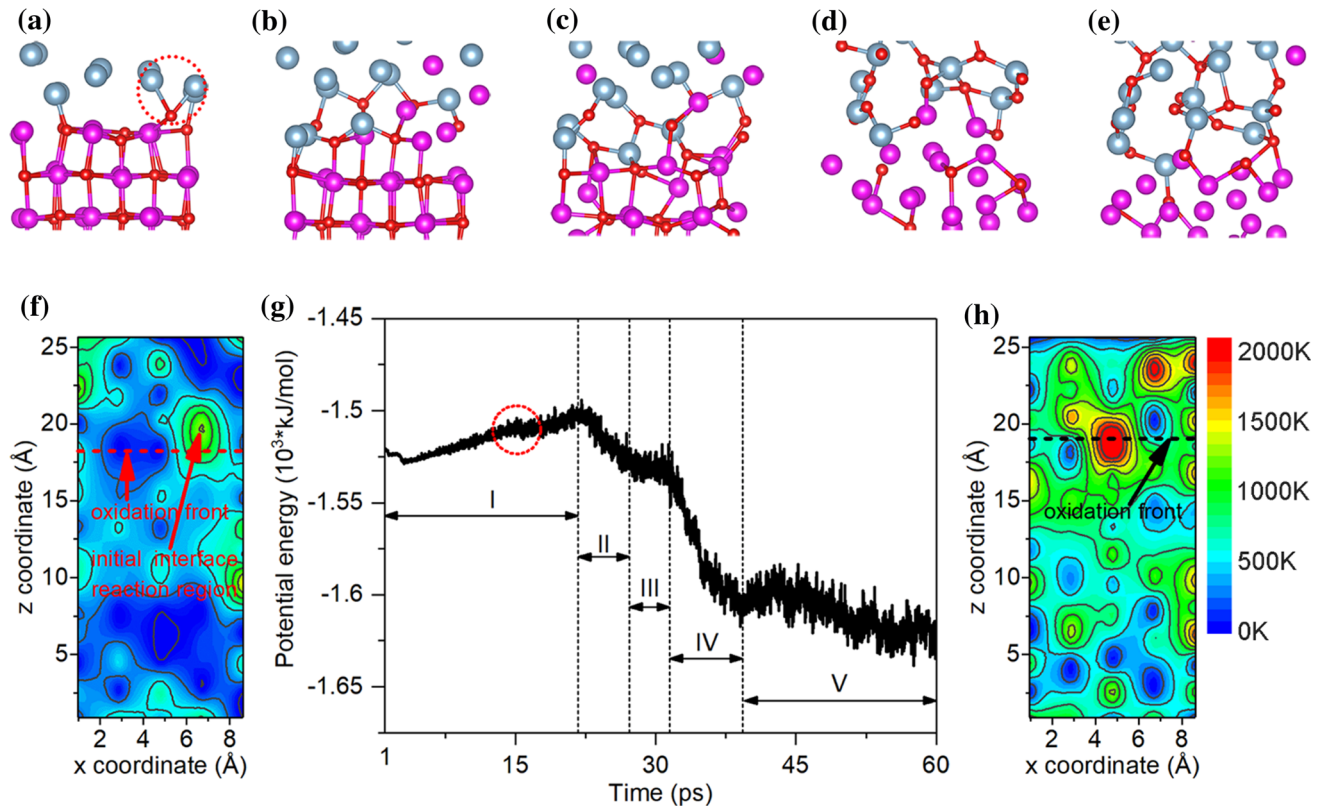
Figure 3 Potential energy curve of the Al/NiO thermite for 10–1500 K simulation (**g**) and its snapshots of corresponding five reaction stages: **a** initial ignition, **b** II stage, **c** III stage, **d** IV stage, and **e** V stage. Temperature distribution profile for Al/NiO thermite at **f** 15.5 ps and **h** 27 ps. Al, Ni, and O atoms are colored in light blue, purple, and red, respectively.

during the five reaction stages are also calculated and shown in Fig. 5.

The value of $g(r)$ represents the probability of an atom pair appearing near a certain distance value. For convenience, we referred to the areas represented by red dotted rectangular boxes between the two peaks in Fig. 4 and 5 as characteristic ones. Figure 4a shows that the $g(r)$ value of the characteristic area is close to zero, which indicates that a small quantity of the interface Ni–O bonds broke during the I stage. It can be found from Fig. 5a and b that the $g(r)$ values of the characteristic region of the interfacial O–Al and bulk O–Al atom pairs are zero during the I stage, that is, no Al–O bond forms. This means that this stage is the ignition process of the thermite reaction and almost no thermite reaction took place, consistent with the statement in "Potential energy curve" section. We can observe in Fig. 4a that the $g(r)$ value in the characteristic area of the stage II presents a sudden change and almost reaches the maximum. In addition, it can be seen in Fig. 4c that the integrated $g(r)$ value decreases significantly means coordination

environment of the interfacial Ni suddenly changes, which indicates the breaking of the interfacial Ni–O bonds in the II stage. Furthermore, the $g(r)$ value of the characteristic area in Fig. 5a is not zero in the II stage. Therefore, the old Ni–O bonds are broken at the interface, and meanwhile the new Al–O bonds formed. In other words, the thermite reaction of the Al/NiO occurs at the interface.

The $g(r)$ values of the characteristic area in the I, II, and III stages are all zero, as shown in Fig. 5b. This means that the bulk NiO did not participate in the thermite reaction during the I, II, and III stages. As shown in Fig. 4b, the $g(r)$ value of the characteristic area in the III stage increases significantly, revealing that the bulk Ni–O bonds are broken at this stage. In Fig. 4d, the platform representing the coordination number of Ni disappears and the integrated $g(r)$ value does not change much. These indicate that although the lattice of the bulk NiO is destroyed, it did not involve in the thermite reaction, consistent with the results observed in Fig. 5b that the $g(r)$ value of the characteristic region is almost zero. Thus, no
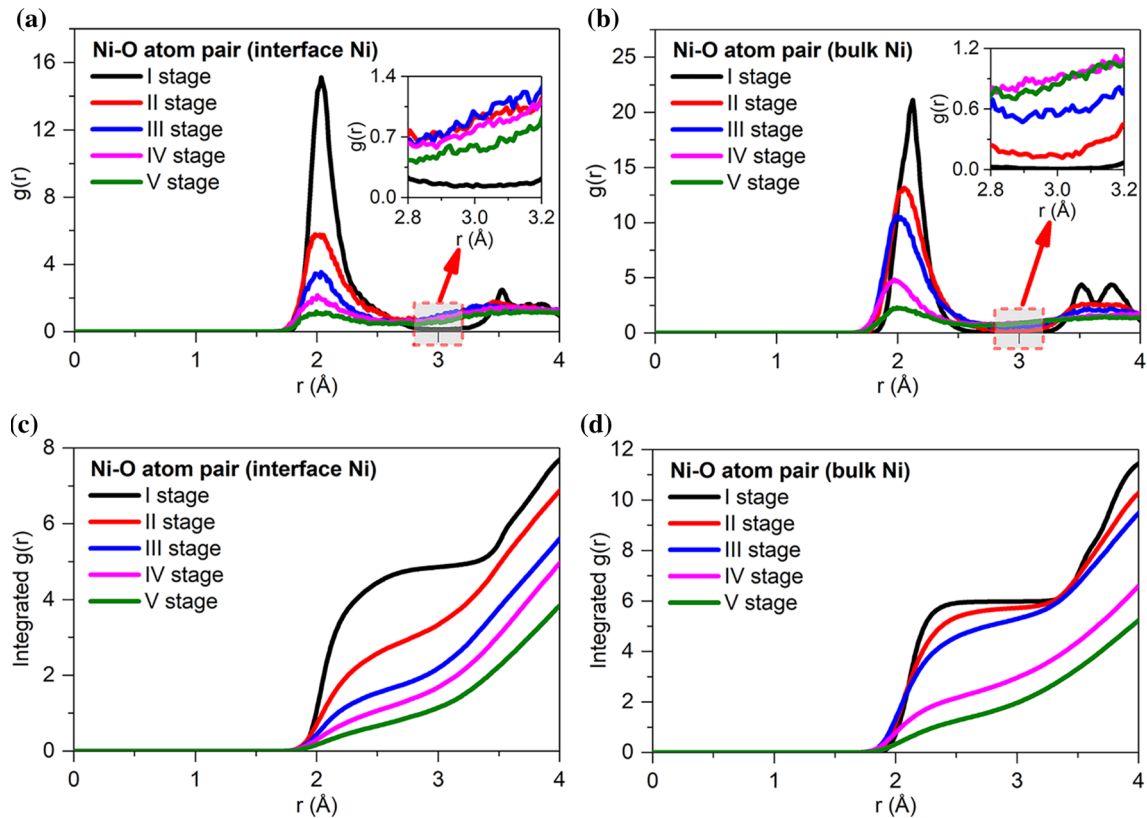
Figure 4 RDF function $g(r)$ of the interfacial Ni–O (a) and bulk Ni–O (b) atom pairs for the Al/NiO thermite and corresponding integrated $g(r)$.
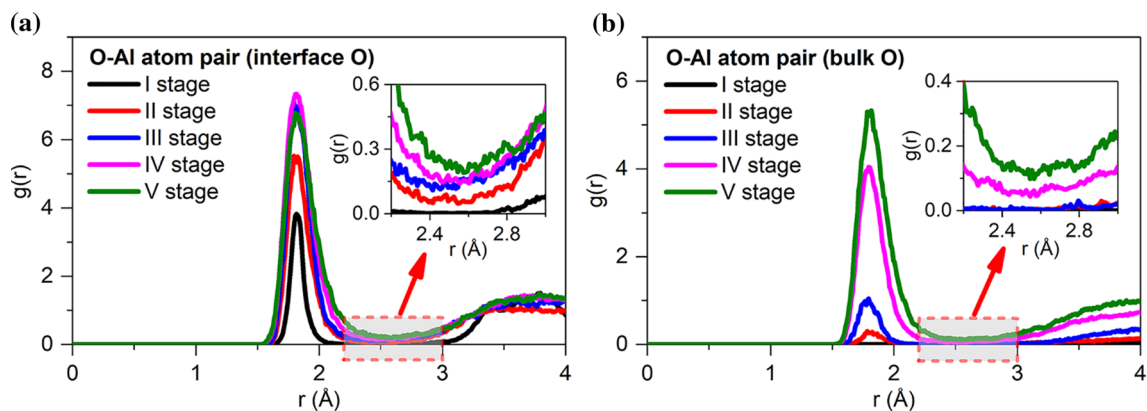

Figure 5 RDF function $g(r)$ of the interfacial O–Al (a) and bulk O–Al (b) atom pairs for the Al/NiO thermite.

new chemical bond formed between the bulk O and all the Al atoms at this stage.

In the IV stage, the $g(r)$ value of the characteristic region in Fig. 4b reaches the maximum, while the integrated $g(r)$ value in Fig. 4d significantly decreases. These indicate the bulk Ni–O bonds are broken. Figure 5b shows that the $g(r)$ value of the characteristic region is not zero, indicating the formation of

bulk O–Al bonds. Thus, the bulk NiO participated in the thermite reaction in the IV stage. In the whole thermite reaction, the $g(r)$ peak value of the first peak of Ni–O atom pair decreases gradually, while that of the Al–O atom pair increases gradually, as shown in Fig. S3. This indicates that the numbers of the Ni–O bonds decrease gradually, while those of the Al–O bonds increase gradually as the thermite reaction

goes on. In sum, the results obtained through the RDF analysis confirm the conclusions drawn from the potential energy curve analysis.

Isotope effect on heat release

Figure 6 compares the potential energy curves of the Al/NiO thermite for the 10–1500 K and 10–1500 K-iso simulations. For the 10–1500 K-iso simulation of the Al/NiO thermite, we also divided the whole reaction process into five stages according to the change of its potential energy. Its each stage is later than corresponding one in the 10–1500 K simulation as provided in Table 1.

We took the temperatures at the beginning of II and III stages as the onset temperature for the twice heating release, respectively. The onset temperature of the initial ignition, primary heat release, and secondary heat release for the Al/NiO thermite increases from 522 to 730 K, 729 to 904 K, and 909 to 1142 K, respectively, as shown in Table 2. The destruction of the bulk NiO lattice took place before the IV stage both in the 10–1500 K and 10–1500 K-iso simulations, which means that it is the precursor process of the rapid chemical reaction stage (IV stage). For the 10–1500 K simulation, the potential energy of the Al/NiO thermite still slightly reduces at III stage, while for the 10–1500 K-iso simulation, a small barrier appears in the potential curve where we marked with a red circle, as shown in Fig. 6. This should be the ^{18}O has a heavier mass and weaker mass transport ability. The reaction progress is
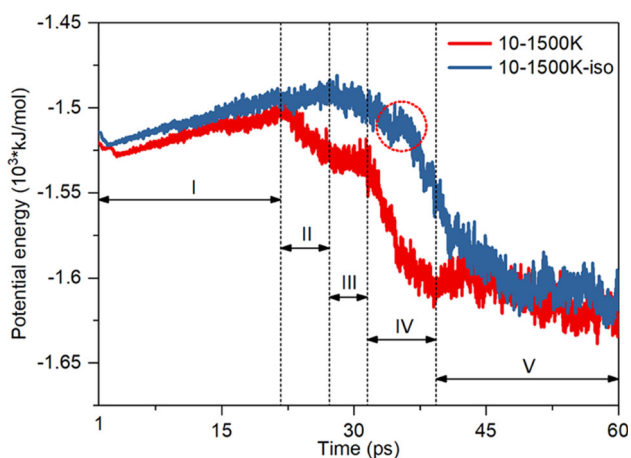
Table 1 Five reaction stages for the Al/NiO thermite in 10–1500 K and 10–1500 K-iso simulations

Stage	Time range (ps)		Reaction mechanisms
	10–1500 K	10–1500 K-iso	
I	0–21.7	0–27.0	Initial ignition
II	21.7–27.2	27.0–34.2	Interface reaction
III	27.2–31.5	34.2–35.6	NiO lattice destruction
IV	31.5–39.3	35.6–48.8	Bulk phase reaction
V	39.3-	48.8-	End of reaction

lagging behind, resulting in a higher potential barrier. These indicate that the weaker oxygen mass transport ability causes a longer delay time, a higher ignition temperature.

In short, the primary heat release during the thermite reaction took place at the interface (II stage) and no bulk NiO participates in this stage. The secondary heat release had a precursor process of the bulk NiO destruction (III stage). Then Al reacted with the original bulk NiO (IV stage) to form a second exothermic peak. Table 2 presents the onset temperature of the two exothermic peaks for the Al/NiO thermite between our simulations and some DSC experiments. It should be noted that we only made a qualitative comparison with experiment results and focused on the overall trend of the reaction due to the limitation of model size and simulation time, although some corresponding numerical values were given based on our simulations. As shown in Fig. 3h, although the average temperature of the system did not reach the melting point of the aluminum phase, the temperature at the oxidation front reached several thousand Kelvin where the aluminum phase has already melted. Furthermore, Puri et al. [50] revealed that the melting point of the Al nanoparticles increases monotonically with the increasing particle size, from 473 K at 2 nm to a bulk value of 937 K at about 8 nm. So the actual thermite reaction is a relatively complicated process. Solid–solid and solid–liquid phase reactions may coexist. According to aforementioned diffusion-controlled mechanism, the reaction between molten Al and NiO can also exhibits secondary heat release. However, this is beyond the scope of this work. In addition, it should be pointed out that many factors, such as heating rate, sample preparation methods, impurities, and the size, thickness, morphology, and equivalent ratios of the

Figure 6 Comparison of potential energy curves for the Al/NiO thermite in the 10–1500 K and 10–1500 K-iso simulations (The five stages of the 10–1500 K simulation are marked in the picture).

Table 2 Onset reaction temperatures of the Al/NiO thermite in different processes

Works	Onset temperature (K)		
	Initial ignition	Primary heat release	Secondary heat release
10–1500 K	522	729	909
10–1500 K-iso	730	904	1142
Exp[a]	–	742	918
Exp[b]	–	774	918
Exp[c]	–	733	839
Exp[d]	–	673	803

[a–d]The experimental data were taken from Refs. [1], [15], [17], and [19] respectively

fuels and oxidants, all affect the onset temperatures, shapes, and even numbers of the exothermic peaks for the nanothermites [1, 19, 21, 51, 52].

Migration of oxygen atoms

In above discussion, the initial ignition at the interface of the nanothermites is related to the migration of oxygen atoms. Meanwhile, the propagation of the thermite reaction is inseparable from the migration of the oxygen atoms. In the experiments, the combustion velocity is usually measured along the vertical direction of a tube [4]. Thus, taking the oxygen atom undergoing an initial ignition at the interface as an object, we studied the migration behaviors of the oxygen atoms in the z direction during the combustion process of the Al/NiO thermite. Figure 7a displays the time evolution of the z coordinates of the O and Al atoms in the Al/NiO thermite. We observed a metal–oxygen flip mechanism which is the position exchange of the O atoms with neighboring Al atoms, while migrating to the z direction [11]. Figure 7b shows the snapshots of the metal–oxygen atomic structure of this position transition in the Al/NiO thermite.

To investigate the migration behaviors of the oxygen atoms in the whole combustion reaction of the Al/NiO thermite, we took the average z coordinates of the oxygen atoms of the first two layers of each interface to study their migration behaviors. The migration distance $z_d(t)$ is defined as:

$$z_d(t) = \frac{\frac{1}{n}\left|\sum_{i=1}^{n} z_i(t) - \sum_{i=1}^{n} z_i(0)\right| + \frac{1}{m}\left|\sum_{j=1}^{m} z_j(t) - \sum_{j=1}^{m} z_j(0)\right|}{2}$$

(1)

where $z_i(t)$ is the z coordination of i-th oxygen atom at the upper interface, $z_j(t)$ is the z coordination of j-th oxygen atom at the lower interface. The letters n and
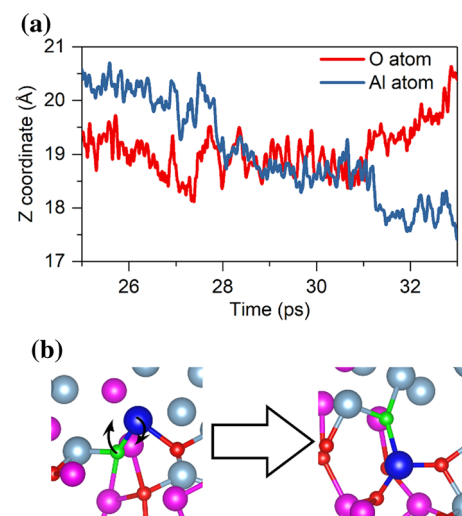

Figure 7 **a** Time evolution of the z coordinate of the oxygen and aluminum atoms that are circled in Fig. 3a and **b** atom configurations of metal–oxygen flip mechanism for the Al/NiO thermite. The light blue and blue spheres are Al atoms, the green and red spheres are O atoms, and the purple spheres are Ni atoms.

m represent the total number of oxygen atoms in the first two layer of upper and lower interfaces respectively. In this paper, the values of n and m are equal to twelve. Figure 8 displays the time evolution of $z_d(t)$ for the Al/NiO thermite. The oxygen migration time in the 10–1500 K simulation is obviously earlier than that in the 10–1500 K-iso simulation. In the early stage, due to the low temperature of the system, only the oxygen atoms at the interface participated in the thermite reaction, resulting in a weak migration. In the rapid reaction stage (IV stage), the migration capacity of the oxygen atoms reaches the maximum. The migration rates of the oxygen atoms for the Al/NiO without and with isotope effect are 22.7 and 20.5 m/s, respectively, as shown in Fig. 8. The former has a slightly higher migration rate than the latter. We can also observe that the longest migration
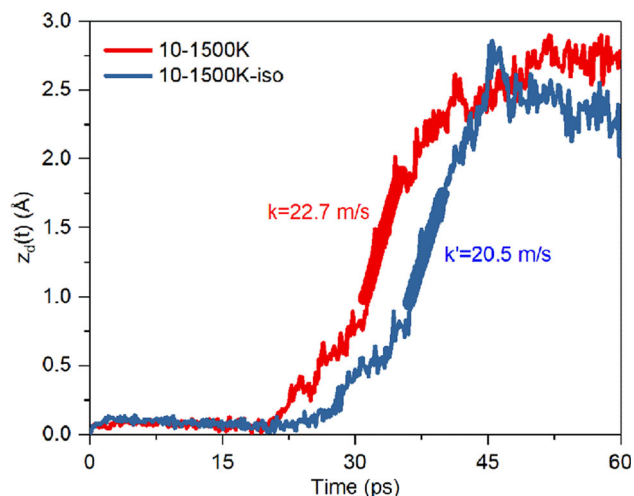
Figure 8 Migration distance $z_d(t)$ of the oxygen atoms in the z direction for the Al/NiO thermite in 10–1500 K and 10–1500 K-iso simulations.

distances about 3 Å of the oxygen atoms in the two simulations are basically the same. However, when the reaction almost completes and tends to equilibrium, the stable migration distances of the oxygen atoms for the former are farther than those for the latter, which may be caused by the lighter atomic mass of the oxygen atom. Therefore, the isotope effect has a significant effect on the migration of the oxygen atoms and then affect the combustion speed of the Al/NiO thermite.

Conclusions

In summary, the ignition and combustion mechanisms and twice exothermic characteristics of the Al/ NiO nanothermite and its isotope effects were investigated by AIMD simulations. It is found that the thermite reaction of Al/NiO can be divided into the five stages: initial ignition (I stage), interface reaction (II stage), NiO lattice destruction (III stage), bulk phase reaction (IV stage), and completion of reaction (V stage).

The initial ignition of the Al/NiO thermite was caused by the migration of the interface O to the Al layer followed by the fracture of the interfacial Ni–O bonds. The twice heat release corresponds to the II and IV stages, respectively. The destruction of the bulk NiO lattice is the precursor process for secondary heat release.

When isotope effects are considered which means the weaker oxygen mass transport ability, the initial ignition time was delayed by about 6.3 ps and the ignition temperature was increased by about 208 K. The maximum oxygen migration rate was reduced from 22.7 to 20.5 m/s. These results indicate that oxygen mass transport capacity has an important influence on the ignition delay and the thermite reaction speed. The metal–oxygen flip mechanism decreases the adverse effect of the oxide film formed in the thermite reaction on the mass transport and ensures the continuous propagation of the thermite reaction.

Declarations

Conflict of interest The authors declare no competing financial interest.

Supplementary Information: The online version contains supplementary material available at http s://doi.org/10.1007/s10853-021-06043-5.

References

[1] Yu CP, Zhang WC, Shen RQ, Xu X, Cheng J, Ye JH, Qin ZC, Chao YM (2016) 3D ordered macroporous NiO/Al nanothermite film with significantly improved higher heat output, lower ignition temperature and less gas production. Mater Des 110:304–310. https://doi.org/10.1016/j.matdes.2 016.08.002

[2] Shimojo F, Nakano A, Kalia RK, Vashishta P (2008) Electronic processes in fast thermite chemical reactions: a first-principles molecular dynamics study. Phys Rev E 77:066103. https://doi.org/10.1103/PhysRevE.77.066103

[3] Plantier KB, Pantoya ML, Gash AE (2005) Combustion wave speeds of nanocomposite Al/Fe$_2$O$_3$: the effects of Fe$_2$O$_3$ particle synthesis technique. Combust Flame 140:299–309. https://doi.org/10.1016/j.combustflame.2004. 10.009

[4] Bockmon BS, Pantoya ML, Son SF, Asay BW, Mang JT (2005) Combustion velocities and propagation mechanisms of metastable interstitial composites. J Appl Phys 98:064903. https://doi.org/10.1063/1.2058175

[5] Petrantoni M, Rossi C, Salvagnac L, Conédéra V, Estève A, Tenailleau C, Alphonse P, Chabal YJ (2010) Multilayered Al/CuO thermite formation by reactive magnetron sputtering: nano versus micro. J Appl Phys 108:084323. https://doi.org/10.1063/1.3498821

[6] Kinsey AH, Slusarski K, Woll K, Gibbins D, Weihs TP (2016) Effect of dilution on reaction properties and bonds formed using mechanically processed dilute thermite foils. J Mater Sci 51:5738–5749. https://doi.org/10.1007/s10853-016-9876-9

[7] Martirosyan KS (2011) Nanoenergetic gas-generators: principles and applications. J Mater Chem 21:9400–9405. https://doi.org/10.1039/C1JM11300C

[8] Jian GQ, Liu L, Zachariah MR (2013) Facile aerosol route to hollow CuO spheres and its superior performance as an oxidizer in nanoenergetic gas generators. Adv Funct Mater 23:1341–1346. https://doi.org/10.1002/adfm.201202100

[9] Staley CS, Raymond KE, Thiruvengadathan R, Apperson SJ, Gangopadhyay K, Swaszek SM, Taylor RJ, Gangopadhyay S (2013) Fast-impulse nanothermite solid-propellant miniaturized thrusters. J Propuls Power 29:1400–1409. https://doi.org/10.2514/1.B34962

[10] Zhang DX, Li XM (2015) Fabrication and kinetics study of nano-Al/NiO thermite film by electrophoretic deposition. J Phys Chem A 119:4688–4694. https://doi.org/10.1021/jp5129113

[11] Shimojo F, Nakano A, Kalia RK, Vashishta P (2009) Enhanced reactivity of nanoenergetic materials: a first-principles molecular dynamics study based on divide-and-conquer density functional theory. Appl Phys Lett 95:043114. https://doi.org/10.1063/1.3189143

[12] Lanthony C, Guiltat M, Ducere JM, Verdier A, Hemeryck A, Djafari-Rouhani M, Rossi C, Chabal YJ, Esteve A (2014) Elementary surface chemistry during CuO/Al nanolaminate-thermite synthesis: copper and oxygen deposition on aluminum (111) surfaces. ACS Appl Mater Interfaces 6:15086–15097. https://doi.org/10.1021/am503126k

[13] Bohlouli-Zanjani G, Wen JZ, Hu A, Persic J, Ringuette S, Zhou YN (2013) Thermo-chemical characterization of a Al nanoparticle and NiO nanowire composite modified by Cu powder. Thermochim Acta 572:51–58. https://doi.org/10.1016/j.tca.2013.09.026

[14] Fischer SH, Grubelich MC (1998) Theoretical energy release of thermites, intermetallics, and combustible metals. https://doi.org/10.2172/658208

[15] Dean SW, Pantoya ML, Gash AE, Stacy SC, Hope-Weeks LJ (2010) Enhanced convective heat transfer in nongas generating nanoparticle thermites. J Heat Transf 132:111201. https://doi.org/10.1115/1.4001933

[16] Wen JZ, Ringuette S, Bohlouli-Zanjani G, Hu A, Nguyen NH, Persic J, Petre CF, Zhou YN (2013) Characterization of thermochemical properties of Al nanoparticle and NiO nanowire composites. Nanoscale Res Lett 8:184. https://doi.org/10.1186/1556-276X-8-184

[17] Yan YC, Shi W, Jiang HC, Xiong J, Zhang WL, Li YR (2015) Fabrication and characterization of Al/NiO energetic nanomultilayers. J Nanomater 2015:1–6. https://doi.org/10.1155/2015/964135

[18] Sui HT, LeSergent L, Wen JZ (2018) Diversity in addressing reaction mechanisms of nano-thermite composites with a layer by layer structure. Adv Eng Mater 20:1700822. https://doi.org/10.1002/adem.201700822

[19] Zhang KL, Rossi C, Alphonse P, Tenailleau C, Cayez S, Chane-Ching J-Y (2009) Integrating Al with NiO nano honeycomb to realize an energetic material on silicon substrate. Appl Phys A 94:957–962. https://doi.org/10.1007/s00339-008-4875-6

[20] Toupkanloo HA, Fathollahi M (2017) Molecular dynamics simulation of Al/NiO thermite reaction using reactive force field (ReaxFF). Phys Chem Res 5:221–237. https://doi.org/10.22036/PCR.2017.40619

[21] Fathollahi M, Toupkanloo HA (2019) Thermal characterization and kinetic analysis of nano-and micro- Al/NiO thermites: Combined experimental and molecular dynamics simulation study. J Chin Chem Soc 66:909–918. https://doi.org/10.1002/jccs.201800371

[22] Zeng HD, Zhu ZY, Zhang JD, Cheng XL (2017) Diffusion and thermite reaction process of film-honeycomb Al/NiO nanothermite: Molecular dynamics simulations using ReaxFF reactive force field. Chin Phys B 26:056101. https://doi.org/10.1088/1674-1056/26/5/056101

[23] Rai A, Park K, Zhou L, Zachariah MR (2006) Understanding the mechanism of aluminium nanoparticle oxidation. Combust Theory Model 10:843–859. https://doi.org/10.1080/13647830600800686

[24] Chowdhury S, Sullivan K, Piekiel N, Zhou L, Zachariah MR (2010) Diffusive vs explosive reaction at the nanoscale. J Phys Chem C 114:9191–9195. https://doi.org/10.1021/jp906613p

[25] Henz BJ, Hawa T, Zachariah MR (2010) On the role of built-in electric fields on the ignition of oxide coated nanoaluminum: ion mobility versus Fickian diffusion. J Appl Phys 107:024901. https://doi.org/10.1063/1.3247579

[26] Levitas VI, Asay BW, Son SF, Pantoya M (2006) Melt dispersion mechanism for fast reaction of nanothermites. Appl Phys Lett 89:071909. https://doi.org/10.1063/1.2335362

[27] Levitas VI, Asay BW, Son SF, Pantoya M (2007) Mechanochemical mechanism for fast reaction of

metastable intermolecular composites based on dispersion of liquid metal. J Appl Phys 101:083524. https://doi.org/10.1063/1.2720182

[28] Levitas VI (2009) Burn time of aluminum nanoparticles: Strong effect of the heating rate and melt-dispersion mechanism. Combust Flame 156:543–546. https://doi.org/10.1016/j.combustflame.2008.11.006

[29] Stamatis D, Jiang Z, Hoffmann VK, Schoenitz M, Dreizin EL, Dense F (2008) Aluminum-rich Al–CuO nanocomposite powders for energetic formulations. Combust Sci Technol 181:97–116. https://doi.org/10.1080/00102200802363294

[30] Tang CM, Chen XX, Cheng XL, Zhang CY, Lu ZP (2018) Ab initio molecular dynamics study of thermite reaction at Al and CuO nano-interfaces at different temperatures. Chem Phys Lett 699:171–181. https://doi.org/10.1016/j.cplett.2018.03.047

[31] Xiong GL, Yang CH, Feng SH, Zhu WH (2020) Ab initio molecular dynamics studies on the transport mechanisms of oxygen atoms in the adiabatic reaction of Al/CuO nanothermite. Chem Phys Lett 745:137278. https://doi.org/10.1016/j.cplett.2020.137278

[32] Xiong GL, Yang CH, Zhu WH (2018) Interface reaction processes and reactive properties of Al/CuO nanothermite: an ab initio molecular dynamics simulation. Appl Surf Sci 459:835–844. https://doi.org/10.1016/j.apsusc.2018.08.069

[33] Blöchl PE (1994) Projector augmented-wave method. Phys Rev B 50:17953–17979. https://doi.org/10.1103/PhysRevB.50.17953

[34] Kresse G, Furthmüller J (1996) Efficient iterative schemes for ab initio total-energy calculations using a plane-wave basis set. Phys Rev B 54:11169–11186. https://doi.org/10.1103/PhysRevB.54.11169

[35] Kresse G, Furthmüller J (1996) Efficiency of ab-initio total energy calculations for metals and semiconductors using a plane-wave basis set. Comput Mater Sci 6:15–50. https://doi.org/10.1016/0927-0256(96)00008-0

[36] Perdew JP, Burke K, Ernzerhof M (1996) Generalized gradient approximation made simple. Phys Rev Lett 77:3865–3868. https://doi.org/10.1103/PhysRevLett.77.3865

[37] Dudarev SL, Botton GA, Savrasov SY, Humphreys CJ, Sutton AP (1998) Electron-energy-loss spectra and the structural stability of nickel oxide: an LSDA+ U study. Phys Rev B 57:1505–1509. https://doi.org/10.1103/PhysRevB.57.1505

[38] Zhao W, Bajdich M, Carey S, Vojvodic A, Nørskov JK, Campbell CT (2016) Water dissociative adsorption on NiO(111): energetics and structure of the hydroxylated surface. ACS Catal 6:7377–7384. https://doi.org/10.1021/acscatal.6b01997

[39] Wang L, Maxisch T, Ceder G (2006) Oxidation energies of transition metal oxides within the GGA+U framework. Phys Rev B 73:195107. https://doi.org/10.1103/PhysRevB.73.195107

[40] Oliver PM, Parker SC, Mackrodt WC (1993) Computer simulation of the crystal morphology of NiO. Model Simul Mat Sci Eng 1:755–760. https://doi.org/10.1088/0965-0393/1/5/015

[41] Arrouvel C, Sanches SG, Werckmann J, Eon J-G (2019) A theoretical and experimental study of the NiO nanocatalyst reactivity. Appl Surf Sci 478:398–407. https://doi.org/10.1016/j.apsusc.2019.01.253

[42] Mei Z, Li CF, Zhao FQ, Xu SY, Ju XH (2019) Reactive molecular dynamics simulation of thermal decomposition for nano-AlH_3/TNT and nano-AlH_3/CL-20 composites. J Mater Sci 54:7016–7027. https://doi.org/10.1007/s10853-019-03364-4

[43] Hoover WG (1985) Canonical dynamics: equilibrium phase-space distributions. Phys Rev A 31:1695–1697. https://doi.org/10.1103/PhysRevA.31.1695

[44] Nosé S (1984) A unified formulation of the constant temperature molecular dynamics methods. J Chem Phys 81:511–519. https://doi.org/10.1063/1.447334

[45] Nosé S (1991) Constant temperature molecular dynamics methods. Prog Theor Phys Suppl 103:1–46. https://doi.org/10.1143/PTPS.103.1

[46] Momma K, Izumi F (2011) VESTA3 for three-dimensional visualization of crystal, volumetric and morphology data. J Appl Crystallogr 44:1272–1276. https://doi.org/10.1107/S0021889811038970

[47] Humphrey W, Dalke A, Schulten K (1996) VMD: visual molecular dynamics. J Mol Graph 14:33–38. https://doi.org/10.1016/0263-7855(96)00018-5

[48] Wang V, Xu N, Liu JC, Tang G, Geng WT (2019) VASPKIT: a user-friendly interface facilitating high-throughput computing and analysis using VASP code. ArXiv190808269. https://arxiv.org/abs/1908.08269

[49] Budka JW, Stan K, Onderka B, Nowak R, Sobczak N (2014) Microstructure, chemistry and thermodynamics of Al/NiO couples obtained at 1273 K. J Alloy Compd 615:S178–S182. https://doi.org/10.1016/j.jallcom.2014.01.056

[50] Puri P, Yang V (2007) Effect of particle size on melting of aluminum at nano scales. J Phys Chem C 111:11776–11783. https://doi.org/10.1021/jp0724774

[51] Yu CP, Zhang WC, Guo SY, Hu B, Zheng ZL, Ye JH, Zhang SL, Zhu JW (2019) A safe and efficient liquid–solid synthesis for copper azide films with excellent electrostatic stability. Nano Energy 66:104135. https://doi.org/10.1016/j.nanoen.2019.104135

[52] Ohkura Y, Liu SY, Rao PM, Zheng XL (2011) Synthesis and ignition of energetic CuO/Al core/shell nanowires. Proc Combust Inst 33:1909–1915. https://doi.org/10.1016/j.proci.2010.05.048